

# A *Chandra* detection of the radio hotspot of 3C 123

M.J. Hardcastle, M. Birkinshaw and D.M. Worrall

*Department of Physics, University of Bristol, Tyndall Avenue, Bristol BS8 1TL*

2 December 2024

## ABSTRACT

*Chandra X-ray Observatory* observations of the powerful, peculiar radio galaxy 3C 123 have resulted in an X-ray detection of the bright eastern hotspot, with a 1-keV flux density of  $\sim 5$  nJy. The X-ray flux and spectrum of the hotspot are consistent with the X-rays being inverse-Compton scattering of radio synchrotron photons by the population of electrons responsible for the radio emission ('synchrotron self-Compton emission') if the magnetic fields in the hotspot are close to their equipartition values. 3C 123 is thus the third radio galaxy to show X-ray emission from a hotspot which is consistent with being in equipartition. *Chandra* also detects emission from a moderately rich cluster surrounding 3C 123, with  $L_X(2 - 10 \text{ keV}) = 2 \times 10^{44} \text{ ergs s}^{-1}$  and  $kT \sim 5 \text{ keV}$ , and absorbed emission from the active nucleus, with an inferred intrinsic column density of  $1.7 \times 10^{22} \text{ cm}^{-2}$  and an intrinsic 2–10 keV luminosity of  $10^{44} \text{ ergs s}^{-1}$ .

**Key words:** galaxies: active – X-rays: galaxies – galaxies: individual: 3C 123 – radiation mechanisms: non-thermal

## 1 INTRODUCTION

The magnetic field strengths in the extended components of extragalactic radio sources cannot be inferred directly from observations of synchrotron emission, and so the energy densities and pressures in the radio-emitting components are poorly constrained. In order to make progress it is common to estimate 'minimum energy' field strengths (Burbidge 1956), which minimise the energy density required for a given synchrotron emissivity. This is roughly equivalent to the assumption that that magnetic and relativistic particle energy densities are equal ('equipartition'). But without measurements of magnetic field strengths these assumptions, for which there is no physical justification, may underestimate the true energy densities by arbitrary factors.

The magnetic field strength may be measured by observations of the 'synchrotron self-Compton' (SSC) process, in which the synchrotron-emitting electrons inverse-Compton scatter synchrotron photons up to X-ray energies. Because the emissivity from this process depends on the photon number density (which is known from radio observations) and the electron number density as a function of energy, observations of SSC emission allow the electron number density to be inferred, and so determine the magnetic field strength. Such tests require observations of regions with well-measured volume and a well-defined synchrotron spectrum with a high photon energy density; these conditions exist in the hotspots of FRII radio sources. Direct evidence supporting the equipartition/minimum energy assumptions in hotspots has come from only two X-ray observations. Harris, Carilli & Perley (1994) detected the hotspots of the powerful FRII Cygnus A (3C 405) with *ROSAT* and showed that the X-ray emission could be interpreted as being due to the SSC process, with a magnetic field strength consistent

with the equipartition model. [This result was recently confirmed with *Chandra* by Wilson, Young & Shopbell (2000).] *ROSAT* was not sensitive enough to detect any other SSC hotspots, though it was used to put lower limits on the field strengths in some sources (Hardcastle, Birkinshaw & Worrall 1998). More recently, *Chandra* verification observations have detected the hotspots of 3C 295, another powerful radio galaxy, at a level which implies field strengths fairly close to the equipartition values if the emission process is SSC (Harris et al. 2000). Here we report a third detection, of the E hotspot of the radio galaxy 3C 123, based on our *Chandra* AO1 guest observer (GO) observations.

3C 123 is a  $z = 0.2177$  radio galaxy, notable for its peculiar radio structure. Like normal classical double sources it has twin hot spots on either side of the active nucleus, but the lobes take the form of diffuse twisted plumes unlike those in any other well-studied object (e.g. Riley & Pooley 1978; Hardcastle et al. 1997, hereafter H97). Like Cygnus A and 3C 295, its radio luminosity is unusually high for its redshift. For our purposes, its most important feature is its bright eastern double hotspot. With a flux density of  $\sim 6$  Jy at 5 GHz, it is the second brightest hotspot complex known (after Cygnus A). The hotspots' structure and synchrotron spectrum are well known (H97; Meisenheimer et al. 1989; Meisenheimer, Yates & Röser 1997; Looney & Hardcastle, 2000).

Throughout this letter we use  $H_0 = 50 \text{ km s}^{-1} \text{ Mpc}^{-1}$  and  $q_0 = 0$ . At the redshift of 3C 123, 1 arcsec corresponds to 4.74 kpc.

## 2 OBSERVATIONS

We observed 3C 123 with the *Chandra X-ray Observatory* for 46.7 ks on 2000 March 21. The source was near the aim point for the

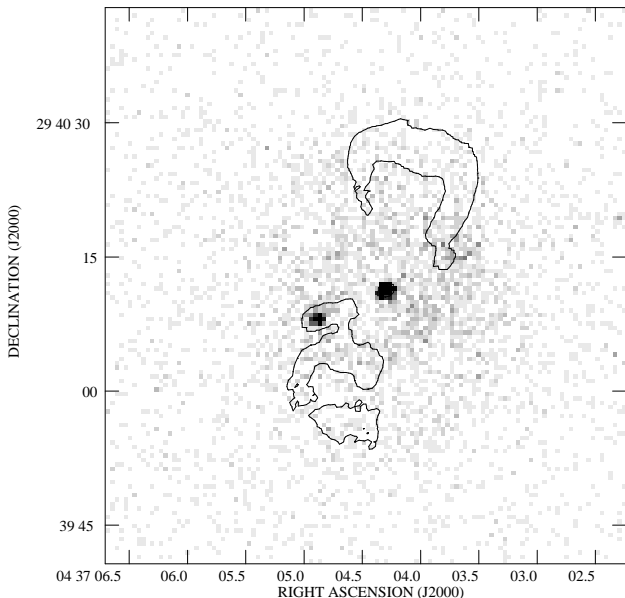


**Figure 1.** Exposure-corrected 0.5–7.0 keV *Chandra* image of the central region of 3C 123. Linear greyscale: black is  $4 \times 10^{-7}$  photons  $\text{cm}^{-2} \text{s}^{-1}$  per standard Chandra pixel (0.492 arcsec on a side). Superposed is the 3 mJy beam $^{-1}$  contour from an 8.4-GHz Very Large Array (VLA) map with 0.6-arcsec resolution (H97), showing the position of the radio lobes. As discussed in section 4, the radio map has been shifted by  $\sim 3$  arcsec so that the radio core aligns with the X-ray nucleus.

S3 ACIS chip. After filtering for intervals of high background, the usable exposure time was 38.5 ks. We considered events in the energy range 0.5–7.0 keV, as the spectral response of the instrument is uncertain outside this range. Fig. 1 shows the exposure-corrected *Chandra* image of 3C 123 in this band. Diffuse cluster emission, an X-ray nucleus and the eastern hotspot are all detected in X-rays. We discuss each component in turn. In each case, spectra were extracted using CIAO, with the best available responses being constructed for each extraction region, and analysed using XSPEC. Spectra were binned such that every bin had  $> 20$  net counts.

### 3 THE CLUSTER

The X-ray counts from 3C 123 are dominated by diffuse cluster-scale emission, which is detectable above the background more than an arcminute away from the central source. The source was known to be extended from *ROSAT* images (Hardcastle & Worrall 1999), and there are many faint optical objects in the field of 3C 123 which may be cluster members (e.g. Longair & Gunn 1975), though strong galactic reddening (the source is at  $b \approx -12^\circ$ , and see below) means that this cluster has not been studied in detail in the optical. We detect around 5,000 counts in a 75-arcsec radius circle centred on the nucleus, excluding the core and hotspot. The overall spectrum of this region is well fitted with an absorbed MEKAL spectrum with  $kT = 5.0^{+0.6}_{-0.4}$  keV, abundance of  $0.47^{+0.12}_{-0.11}$  solar and a galactic hydrogen column density of  $4.3^{+0.2}_{-0.3} \times 10^{21} \text{ cm}^{-2}$  (errors are  $1\sigma$  for one interesting parameter). 3C 123 lies behind a well-known molecular cloud system in Taurus (e.g. Ungerechts & Thaddeus 1987), and our derived column density is consistent with the total hydrogen column inferred from radio observations of the molecular cloud system. From HI absorption against 3C 123, Col-

gan, Salpeter & Terzian (1988) derive  $N_{\text{HI}} = 1.97 \times 10^{21} \text{ cm}^{-2}$  at the velocity of the cloud system, while the molecular hydrogen column can be inferred from CO measurements [ $W_{\text{CO}} \approx 10 \text{ K km s}^{-1}$ , Megeath (private communication)] to be  $N_{\text{H}_2} \approx 1.6 \times 10^{21} \text{ cm}^{-2}$ , with a large systematic uncertainty [we use a recent estimate of the conversion factor averaged over the galactic plane, due to Hunter et al. (1997), but this may not be appropriate for the Taurus region]. We adopt a galactic absorption column of  $4.3 \times 10^{21} \text{ cm}^{-2}$ , unless otherwise stated, from now on.

The X-ray spectral fit implies a rest-frame 2–10 keV luminosity from the cluster within a radius of 75 arcsec (360 kpc) of  $2 \times 10^{44} \text{ ergs s}^{-1}$ , consistent with the fitted temperature on the temperature-luminosity relation (determined largely for Abell clusters) of David et al. (1993). Fig. 1 shows a plateau of X-ray emission on scales comparable to those of the radio source, with clear structure in the emission (note particularly X-ray voids to the E and SW of the nucleus) although there is no evidence for interaction between the X-ray gas and the radio lobes. The voids may represent large-scale inhomogeneity in the cluster gas; if so, they would help to explain the peculiar radio structure. The central cooling time is a few  $\times 10^9$  years, so we might expect to see a cooling flow around the source. But there is no strong evidence for cooling in the temperature fits; the best-fitting temperature for the material within 15 arcsec of the nucleus (fixing the abundance to the value obtained for the whole cluster) is  $4.4 \pm 0.3$  keV. Since gas with temperatures below  $\sim 3$  keV is not observed even in the centres of well-studied cooling flows (e.g. Fabian et al. 2000, Peterson et al. 2000) this is perhaps not surprising. Our preliminary analysis implies particle densities around the lobes which are similar to those reported by Hardcastle & Worrall (2000) using *ROSAT* data, and the measured temperature implies comparable, but slightly larger, external pressures.

### 4 THE NUCLEUS

The point-like nucleus contains  $517 \pm 36$  0.5–7.0 keV counts, measured in a 2.5-arcsec region about the centroid, with the background being taken from a 3–5 arcsec concentric annulus. Pileup is not significant. The X-ray core position (J2000.0) is measured to be 04 37 04.30 +29 40 11.2. The core position measured from the VLA radio map of H97 is 04 37 04.375 +29 40 13.86, and this is expected to be accurate to within about 0.05 arcsec. The X-ray core position is therefore offset from the (true) radio position by about 3 arcsec. We attribute this to uncertainties in aspect determination in the early version of the pipeline software (R4CU4UPD7.4) used to process the *Chandra* data (see URL: <<http://asc.harvard.edu/mta/ASPECT/>>). In Fig. 1 we have aligned the radio data with the X-ray core.

The spectrum of the nucleus is well fitted with an absorbed, flat-spectrum power law model. Fitting with free galactic absorption, the best-fit values of photon index  $\Gamma$  and  $N_{\text{H}}$  are  $1.16 \pm 0.14$  and  $1.48^{+0.32}_{-0.24} \times 10^{22} \text{ cm}^{-2}$ , respectively. If we fix galactic absorption at the value derived from the cluster fits and require the absorber to be at the redshift of the galaxy, the best-fit  $N_{\text{H}}$  for the intrinsic absorber is  $1.69^{+0.51}_{-0.41} \times 10^{22} \text{ cm}^{-2}$ , with the photon index unchanged. This implies a rest-frame 2–10 keV luminosity (assumed isotropic) of  $10^{44} \text{ ergs s}^{-1}$ , comparable to the luminosity of the nuclear component in 3C 295 (Harris et al. 2000). Fits in which the absorbing column is constrained to the galactic value are much poorer and require an inverted nuclear spectrum. The column density required for the intrinsic absorber is considerably lower than

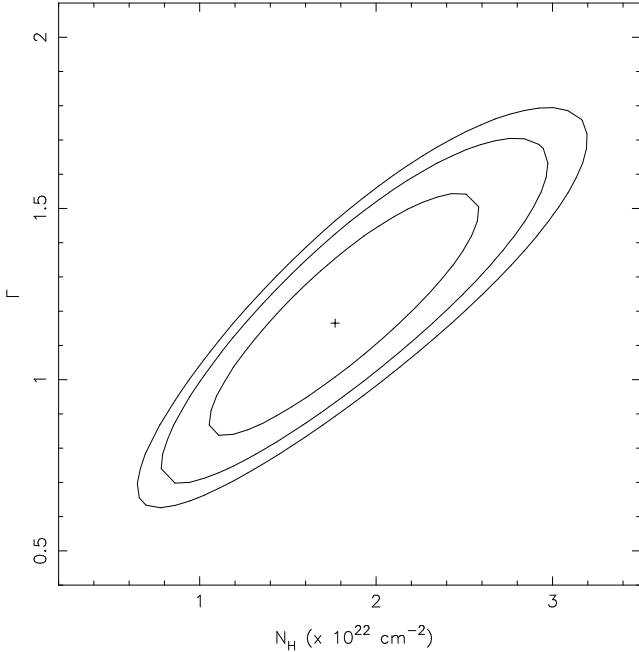


**Figure 2.** Joint confidence contours for the spectrum of the nucleus of 3C 123 using the model described in the text. Intrinsic absorbing column is plotted on the  $x$ -axis, power-law photon index on the  $y$ -axis. The contours are at 1, 2 and  $3\sigma$  for two interesting parameters. The cross marks the best-fit values.

the  $4 \times 10^{23} \text{ cm}^{-2}$  inferred for Cygnus A by Ueno et al. (1994), and more comparable to that inferred for the much lower luminosity nucleus of Hydra A by Sambruna et al. (2000). The best-fit photon index is flatter than might be expected from, for example, the photon indices of radio-loud quasars (e.g. Lawson & Turner 1997) or other radio galaxies (Sambruna, Eracleous & Mushotzky 1999) although the errors are large; as shown in Fig. 2, more reasonable values of  $\Gamma$  are allowed in conjunction with somewhat higher intrinsic absorbing columns. The inferred absorbing column in front of the nucleus explains the non-detection of this core component in the *ROSAT* HRI image (Hardcastle & Worrall 1999).

## 5 THE HOTSPOT

The E hotspot complex is detected with  $145 \pm 32$  0.5–7.0 keV counts, using a 2.5-arcsec source circle and concentric 3–5 arcsec background annulus. The X-ray hotspot is positionally coincident with the larger, ‘secondary’ hotspot of the eastern hotspot pair in the radio (after the X-ray and radio cores have been aligned). The X-ray emission appears to be slightly elongated in an east-west direction, matching the radio. (The X-ray structure will be discussed in more detail in a subsequent paper which will include results of further radio observations now in progress.) The X-ray spectrum of the hotspot is well fitted with a power law with  $\Gamma = 1.6 \pm 0.3$ , with the absorbing column fixed at the galactic value. The corresponding unabsorbed 1-keV flux density is  $4.6 \pm 0.9$  nJy.

We used the synchrotron-self-Compton code described by Hardcastle et al. (1998) to predict the SSC flux density expected at this frequency from the hotspots. The basic model for the hotspots is described by Looney & Hardcastle (2000). The larger hotspot is treated as a cylinder of  $1.14 \times 0.54$  arcsec (length times radius); the fainter ‘primary’ (more compact) hotspot is a cylinder

of  $0.74 \times 0.14$  arcsec, based on the MERLIN maps of H97. Radio flux densities of the two components are taken from Looney & Hardcastle. In addition to these, we have used infra-red and optical upper limits and a 231-GHz data point from Meisenheimer et al. (1989, 1997) and archival HST observations, and low-frequency radio data from Readhead & Hewish (1974) and Stephens (1987). As these data do not resolve the two hotspot components, we have *approximately* corrected them by scaling by the appropriate factors measured from the 5-GHz data. Looney & Hardcastle showed that the radio-to-mm spectra of the two hotspots are well modelled as broken power laws, and we adopt the break energies they found. The apparent low-frequency turnover in the spectrum observed by Stephens (1987) requires a low-energy cutoff in the electron energy spectrum corresponding at equipartition to a minimum Lorentz factor  $\gamma_{\min} \approx 1000$ , and we adopt this value, although Stephens’ flux densities are inconsistent with a larger flux at a lower frequency derived from the scintillation measurements of Readhead & Hewish. If we were to adopt the scintillation measurements as our low-frequency constraint, we would obtain  $\gamma_{\min} \approx 400$ , which is more consistent with the value inferred for the hotspots of Cygnus A by Carilli et al. (1991); but this would not significantly affect our conclusions. (Scheduled low-frequency VLBA observations should give a definitive answer.) An upper limit on the maximum Lorentz factor is given by the non-detection in the IR,  $\gamma_{\max} < 3.6 \times 10^5$ ; a lower limit is given by the detection at 231 GHz,  $\gamma_{\max} > 8 \times 10^4$ . The SSC emissivity at 1 keV turns out to be insensitive to  $\gamma_{\max}$  if it lies between these two values, and so we fix  $\gamma_{\max}$  at its largest value. With these parameters, the equipartition field strengths of the two eastern hotspot components, assuming no contribution to the energy density from non-radiating particles such as protons, are 24 nT (primary) and 16 nT (secondary), and the predicted SSC flux densities at 1 keV are respectively 0.44 and 2.6 nJy. The predicted photon index at this frequency is 1.55 (of course, this is simply a function of the electron energy spectrum, and so is true for any inverse-Compton process). Fig. 3 shows the synchrotron fluxes and SSC prediction for the secondary hotspot. The predicted SSC flux density for the much weaker western hotspot pair is negligible,  $\sim 0.07$  nJy, corresponding to 2 *Chandra* counts in this observation.

These predictions are relatively insensitive to cosmological parameters; for example, using a cosmology where  $\Omega_{\text{matter}} = 1.0$  gives a 3 per cent decrease in the expected flux density from the secondary, while using  $H_0 = 70 \text{ km s}^{-1} \text{ Mpc}^{-1}$ ,  $\Omega_{\text{matter}} = 0.3$ ,  $\Omega_{\Lambda} = 0.7$  gives a 2 per cent decrease. The hotspots may be projected, but this also has only a weak effect: if the projection angle is  $45^\circ$  then the true long axis is larger by a factor  $\sqrt{2}$  and the predicted flux is about 7 per cent lower. One clear systematic error in the calculations comes from an assumption of spherical symmetry for the scattering geometry which is used in the SSC code. Because a cylinder has a higher surface area to volume ratio, the mean photon density is lower in a cylinder than in a sphere for a given volume synchrotron emissivity. We estimate that this effect is less than 10 per cent for the secondary component, but we may be overestimating the SSC flux from the fainter primary by 30 per cent (these values are increased if there is substantial projection).

Comparing our predicted flux densities with the data, we see that the magnitude of the observed flux density, its origin in the larger eastern hotspot and its photon index are all in good agreement with the equipartition predictions of the SSC model, as is the non-detection of the western hotspot pair. The observed 1-keV flux density of the E hotspots is somewhat higher than the predicted value for an equipartition field, though only by about 1.5 standard deviations. Most of the changes to the model discussed above have

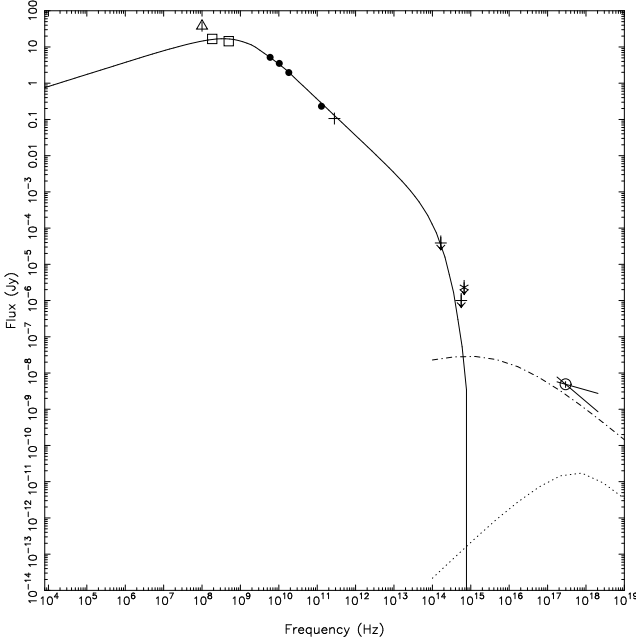


**Figure 3.** The spectrum of the secondary hotspot of 3C 123 at equipartition. Points are from data as described in the text. Symbols indicate the source of the data, as follows: filled circles, Looney & Hardcastle (2000); crosses, Meisenheimer et al. (1989); triangle, Readhead & Hewish (1974); star, optical limit from HST data; open circle, *Chandra* data point. Arrows denote an upper limit. Error bars are smaller than the symbols in most cases. The solid line is the model synchrotron spectrum. The dash-dotted line shows the predicted SSC spectrum at equipartition and the dotted line shows inverse-Compton emission due to scattering of microwave background photons. The two solid bars through the X-ray data point show the 0.5–7.0 keV band of the *Chandra* data and the  $1\sigma$  range of photon indices permitted by the data. Frequencies are plotted in the rest frame of the radio source.

the effect of reducing the SSC flux density; to increase it we must reduce the magnetic field strength or find an additional (external) source of photons. If the magnetic field in the secondary hotspot is reduced by 25 per cent to 12 nT, the secondary can produce all the flux seen in X-rays. Neglecting the small SSC contribution from the primary hotspot, the *Chandra* data with their associated uncertainties imply within the SSC model that the magnetic field strength in the secondary hotspot is  $12 \pm 2$  nT ( $1\sigma$  statistical errors only).

One possible external source of photons is the active nucleus of 3C 123. Inverse-Compton (IC) scattering of photons from the active nucleus will make a significant contribution to the X-ray emission if such photons (at frequencies around  $10^{11}$  Hz, since  $\gamma_{\min} \approx 1000$ ) are comparable in number density to the synchrotron photons. At this frequency, the number density of synchrotron photons is approximately  $0.08 \text{ m}^{-3} \text{ Hz}^{-1}$ ; since the hotspots are a projected 37 kpc from the nucleus, a similar number density would be produced from the nucleus if its luminosity at this frequency as seen by the hotspot were  $\gtrsim 2 \times 10^{27} \text{ W Hz}^{-1} \text{ sr}^{-1}$ , which would correspond to a flux density of  $\gtrsim 100 \text{ Jy}$  at  $10^{11}$  Hz. (This condition is equivalent to  $S_{\text{core}} = (3D/2R)^2 S_{\text{hs}}$ , where  $D$  is the core-hotspot distance and  $R$  is the hotspot radius, and the two fluxes are measured at the required frequency.) The observed core flux density of 3C 123 at  $10^{11}$  Hz is about 40 mJy, though it may be variable (Looney & Hardcastle 2000), so that isotropic radiation from the core cannot provide the required photon density. However, if the core emission at this frequency is beamed, the hotspot will see the

core as having a higher luminosity than the one we observe. We assume the most favourable case for this model of no misalignment between the pc- and kpc-scale jet, though such good alignment is not often observed, and we neglect effects due to the finite angle subtended by the hotspot at the nucleus, which may be significant. The ratio of required to observed flux,  $\mathcal{R}$  ( $\mathcal{R} \approx 2500$  for rough equality of predicted SSC and IC flux densities), then constrains  $\beta$ , the bulk speed in the nucleus, and  $\theta$ , the angle of the core-hotspot vector to the line of sight:

$$\frac{(1 - \beta)^{-(2+\alpha)} + (1 + \beta)^{-(2+\alpha)}}{(1 - \beta \cos \theta)^{-(2+\alpha)} + (1 + \beta \cos \theta)^{-(2+\alpha)}} = \frac{(1 - \cos \theta)^{-(1+\alpha)} \mathcal{R}}{\sin^2 \theta}$$

where the term  $(1 - \cos \theta)^{-(1+\alpha)}$  approximately corrects for the anisotropic nature of the resulting IC emission (e.g. Jones, O'Dell & Stein 1974), and the core is treated as a two-sided jet with a power-law spectrum; the  $\sin^2 \theta$  term incorporates the effects of projection. If we assume a core spectral index  $\alpha = 0.5$ , then we can obtain  $\mathcal{R} \approx 2500$  for plausible  $\beta$ , corresponding to bulk Lorentz factors  $\sim 4\text{--}10$ , if the source is within 50 degrees of the plane of the sky. (In reality, this value for  $\alpha$  is probably an overestimate, since the  $10^{11}$  Hz photons seen by the nucleus will be blueshifted from lower frequencies where core spectra are typically flat,  $\alpha \approx 0$ . Lower  $\alpha$  requires higher  $\beta$ .) As no jet has been detected in 3C 123 and its optical emission lines are weak, the angle to the line of sight is not constrained, and so we cannot rule out a contribution to the X-ray emission from nuclear IC scattering. However, a contribution at approximately the same level as the SSC emission would not affect the conclusion that the hotspot is close to equipartition; in fact, it might account for some of the difference between the equipartition prediction and the observed 1-keV flux density. But if nuclear IC emission *dominates* the observed X-rays, then the hotspot could have a magnetic field higher than the equipartition value, and this cannot be ruled out by the present observations. For example,  $\mathcal{R} = 2.5 \times 10^4$ , corresponding to an IC emissivity ten times the SSC value, can be obtained for a bulk Lorentz factor  $\approx 6$  if the source is close to the plane of the sky and  $\alpha = 0.5$ , and would require  $B \approx 4B_{\text{eq}}$ . Such a model requires a coincidence to explain the similarity of the observed emissivity to that predicted by the simple SSC model with a near-equipartition field.

In carrying out the SSC calculations we have assumed that the hotspots are homogeneous, that they contain no relativistic protons, and that the small-scale filling factor is unity. From the MERLIN maps of H97 we know that the hotspots do have internal structure on 100-pc scales, although the variations in surface brightness are not very large; there is no evidence for filamentary structures of the kind seen in radio lobes. As discussed in Hardcastle & Worrall (2000), the general effect of a filling factor less than unity is to increase the SSC emissivity, but the results are dependent on the geometry of the synchrotron-emitting regions, particularly if the low filling factor is a result of a spatial variation in electron density in a relatively constant magnetic field. Our present results may be taken as evidence against low filling factors in the hotspots, as such filling factors would require coincidences to produce X-ray emission at the observed levels. Similarly, if the particle population is energetically dominated by non-synchrotron-emitting particles such as relativistic protons, it is a coincidence that the energy density in magnetic field corresponds so closely to that in the synchrotron-emitting electrons.

Although SSC emission is a required process, we cannot rule out the possibility that the magnetic field strength is much greater than the equipartition value and that some other process happens to produce X-ray emission at a level consistent with the SSC model.

One such process which we have already discussed is the IC scattering of nuclear photons. Some other simple models can be rejected. Thermal bremsstrahlung can be ruled out by the compact structure seen with *Chandra* and the flat X-ray spectrum, while, as shown in Fig. 3, IC scattering of the microwave background is two orders of magnitude too weak to be responsible for the observed emission. But more speculative models remain possible. For example, we cannot rule out the possibility that the X-ray emission is synchrotron radiation from an arbitrarily chosen population of electrons. This model has been invoked to explain some other X-ray hotspots (e.g. Harris et al. 1999) in which the IC or SSC models do not seem to work well. In the case of 3C 123, it requires a coincidence to explain the close similarity between the observed X-ray emission and the predictions of the SSC model.

One model which makes quantitative predictions about the origin and properties of this second population of electrons is the proton-induced cascade (PIC) model of Mannheim, Krülls & Biermann (1991). In this model, the high-energy electrons which produce X-ray synchrotron emission are the end result of photomeson production on a population of ultra-relativistic protons, through pion decay and pair production. If protons are present in the jet, they should undergo shock acceleration in the hotspot; there is some evidence for high-energy protons in the lobes of FRII sources (Leahy & Gizani 1999, Hardcastle & Worrall 2000). Mannheim et al. considered the hotspot of 3C 123 and predicted that the PIC process would dominate over SSC if protons were highly energetically dominant in the hotspot and in equipartition with magnetic fields at the level inferred by Meisenheimer et al. (1989), somewhat higher than our equipartition fields. Their predicted X-ray flux at 1 keV is  $\sim 30$  nJy, nearly a factor 10 higher than the observed value, so a model with extreme proton dominance does not seem to be consistent with the data. However, if protons have energy densities closer to those of the electrons, we cannot rule out an origin from PIC-generated electrons for some or all of the observed X-rays; the spectra of the two processes are not distinguishable with our data. Once again, though, a moderate contribution from the PIC process would not affect our conclusions regarding the closeness of the hotspot to equipartition, while a model in which PIC was responsible for *all* the emission would require fine-tuning of the energy fraction in fields, electrons and protons, and so seems less plausible than the simple SSC model.

## 6 CONCLUSIONS

The X-ray emission from the E hotspot of 3C 123 is consistent with a SSC model, with the inferred magnetic field strength close to the value predicted from equipartition of energy between the magnetic field and the synchrotron-emitting electrons. Other models are possible, but require coincidences to explain the closeness of the X-ray flux density and (in some cases) the photon index to the SSC prediction. This reinforces a conclusion already drawn from observations of Cygnus A and 3C 295 that the magnetic field strengths in typical hotspots are near their equipartition values. Although there is still no *a priori* reason to expect equipartition, it is now very likely that it is achieved in the hotspots of at least some fraction of the source population. Observations of inverse-Compton scattering of microwave background photons from radio lobes may tell a similar story (Feigelson et al. 1995; Tsakiris et al. 1996; Tashiro et al. 1998). Even the deviations from equipartition reported by Tashiro et al. require a magnetic field strength only a factor  $\sim 2$  below the equipartition value. However, some X-ray detections of hotspots

(e.g. 3C 120, Harris et al 1999; Pictor A, Wilson, Young & Shopbell 2001) are at a level much too bright to be consistent either with synchrotron emission (from the electron population responsible for the radio and optical synchrotron radiation) or with SSC at equipartition. More observations are necessary to demonstrate that Cygnus A, 3C 295 and 3C 123 are typical of most radio sources. We will report on the results of scheduled *Chandra* observations of further hotspot sources in a future paper.

## ACKNOWLEDGEMENTS

We thank all those involved with the design and operation of *Chandra* for doing such an excellent job, and particularly the staff of the *Chandra* X-ray Center for their help with data analysis. We are grateful to an anonymous referee for a careful reading of the paper and constructive suggestions. The National Radio Astronomy Observatory Very Large Array is operated by Associated Universities Inc., under co-operative agreement with the National Science Foundation.

## REFERENCES

Burbidge G., 1956, ApJ, 124, 416  
 Carilli C.L., Perley R.A., Dreher J.W., Leahy J.P., 1991, ApJ, 383, 554  
 Colgan S.W.J., Salpeter E.E., Terzian Y., 1988, ApJ, 328, 275  
 David L.P., Slyz A., Jones C., Forman W., Vrtilek S.D., 1993, ApJ, 412, 479  
 Fabian A.C., et al., 2000, MNRAS in press, astro-ph/0007456  
 Hardcastle M.J., Alexander P., Pooley G.G., Riley J.M., 1997, MNRAS, 288, 859 [H97]  
 Hardcastle M.J., Birkinshaw M., Worrall D.M., 1998, MNRAS, 294, 615  
 Hardcastle M.J., Worrall D.M., 1999, MNRAS, 309, 969  
 Hardcastle M.J., Worrall D.M., 2000, MNRAS in press (astro-ph/0007260)  
 Harris D.E., Carilli C.L., Perley R.A., 1994, Nat, 367, 713  
 Harris D.E., Hjorth J., Sadun A.C., Silverman J.D., Vestergaard M., 1999, ApJ, 518, 213  
 Harris D.E., et al., 2000, ApJ, 530, L81  
 Hunter S.D., et al., 1997, ApJ, 481, 205  
 Jones T.W., O'Dell S.L., Stein W.A., 1974, ApJ, 188, 353  
 Lawson A.J., Turner M.J.L., 1997, MNRAS, 288, 920  
 Leahy J.P., Gizani N.A.B., 1999, To appear in 'Life Cycles of Radio Galaxies', ed. J. Biretta et al., New Astronomy Reviews, astro-ph/9909121  
 Longair M.S., et al., 1975, MNRAS, 170, 121  
 Looney L.W., Hardcastle M.J., 2000, ApJ, 534, 172  
 Mannheim K., Krülls P.L., Biermann P.L., 1991, A&A, 251, 723  
 Meisenheimer K., Röser H.-J., Hiltner P.R., Yates M.G., Longair M.S., Chini R., Perley R.A., 1989, A&A, 219, 63  
 Meisenheimer K., Yates M.G., Röser H.-J., 1997, A&A, 325, 57  
 Peterson J.R., et al., 2000, A&A in press, astro-ph/0010658  
 Readhead A.C.S., Hewish A., 1974, Mem. RAS, 78, 1  
 Riley J.M., Pooley G.G., 1978, MNRAS, 183, 245  
 Sambruna R.M., Chartas G., Eracleous M., Mushotzky R.F., Nousek J.A., 2000, ApJ, 532, L91  
 Sambruna R.M., Eracleous M., Mushotzky R.F., 1999, ApJ, 526, 60  
 Stephens P., 1987, PhD thesis, University of Manchester  
 Tashiro M., et al., 1998, ApJ, 499, 713  
 Ueno S., Koyama K., Nishida M., Yamauchi S., Ward M.J., 1994, ApJ, 431, L1  
 Ungerechts H., Thaddeus P., 1987, ApJS, 63, 645  
 Wilson A.S., Young A.J., Shopbell P.L., 2000, ApJ (Letters) in press (astro-ph/0009308)  
 Wilson A.S., Young A.J., Shopbell P.L., 2001, ApJ in press (astro-ph/0008467)

This paper has been produced using the Royal Astronomical Society/Blackwell Science L<sup>A</sup>T<sub>E</sub>X style file.